Journal of Hydrology 411 (2011) 25–36

Contents lists available at SciVerse ScienceDirect

Journal of Hydrology

journal homepage: www.elsevier.com/locate/jhydrol

Multidimensional scaling and inverse distance weighting transform for image processing of hydrogeological structure in rock mass

Yoshitada Mito [a,*], Mohd Ashraf Mohamad Ismail [b], Takuji Yamamoto [c]

[a] Department of Urban Management, Graduate School of Engineering, Kyoto University, Nishikyo-ku, Kyoto 6158530, Japan
[b] School of Civil Engineering, Universiti Sains Malaysia, Engineering Campus, 14300 Nibong Tebal, Seberang Prai Selatan, Pulau Pinang, Malaysia
[c] Kajima Corporation, 19-1, Tobitakyu 2-Chome, Chofu-shi, Tokyo 182-0036, Japan

ARTICLE INFO

Article history:
Received 1 July 2010
Received in revised form 14 August 2011
Accepted 15 September 2011
Available online 8 October 2011
This manuscript was handled by Philippe Baveye, Editor-in-Chief

Keywords:
Preferential flow path
Multidimensional scaling
Inverse distance weighting
Cross-hole hydraulic test

SUMMARY

A new imaging method based on the multidimensional scaling (MDS) and inverse distance weighting (IDW) transform is proposed in this study. This method aims to identify, characterize and process an image of the preferential flow path in a rock mass, which strongly governs the hydraulic behavior of this rock mass. This methodology uses pair-wise hydraulic diffusivity data from cross-hole hydraulic testing as the input data. The input data are then processed by MDS and IDW to generate a spatial distribution map of the hydraulic properties, which can be used to infer the preferential flow path in the rock mass. The reliability of this novel method was validated through numerical experiments using several continuum models with different hydrogeological structures, and the applicability of the developed method to the actual field was verified through in situ experiments.

1. Introduction

The performance of underground facilities such as high-level waste repositories and underground storage caverns depends on the hydraulic behavior of the surrounding rock mass (Chung et al., 2003; Giramonti et al., 1978; Lindblom, 1989; Runchal and Maini, 1980; Tiren et al., 1999). The performance evaluation for such kinds of underground facilities normally focuses on the potential fluid transport from or to the surrounding hydrogeological environment, where the fluid flows are primarily governed by the hydraulic properties of the surrounding rock and the preferential flow paths embedded in the rock mass (Bonin et al., 2000; Kiyoyama, 1990; Kjorholt and Broch, 1992; Zimmerman and Bodvarsson, 1996).

In a rock mass, fluid flow is often concentrated or localized in certain flow paths, which heavily influence hydraulic behavior (Park et al., 2002; Wang and Kulatilake, 2008). Identifying these flow paths is therefore essential. However, knowledge of the presence and the connectivity of the flow paths, especially the super conductive fracture, is generally quite difficult to obtain due to the heterogeneity of the rock mass.

To grasp the heterogeneity of the hydraulic properties of rock masses, various hydraulic tests based on point-wise measurements have been developed, including the Lugeon test, pumping test, slug test and constant head injection test (Black, 1978; Bouwer and Rice, 1976; Butler and Zhan, 2004; Houlsby, 1976; Kipp, 1985; Pickens et al., 1987). These tests deliver point-wise data that require a spatial interpolation to estimate the properties at unsampled sites in the area surrounding the sampled points (Cassiani et al., 1998). However, the hydraulic behavior of a rock mass can vary by several orders of magnitude within the short distances between fractures and the matrix, thus increasing the uncertainty of the interpolation.

In general practice, the most conductive fractures at the borehole scale are identified based on the core logs and borehole television (BTV) observations. Subsequently, intensive packer testing is performed in multiple boreholes, and pressure variations in multiple intervals in the observation boreholes are monitored by the cross-hole hydraulic test (Martinez-Landa and Carrera, 2006). The sequential step is needed because the single borehole only provides information about the properties of the fracture segments surrounding the borehole, whereas the cross-hole hydraulic test provides information on the properties of the flow zones that connect borehole pairs. The pair-wise hydraulic measurements obtained by the cross-hole hydraulic test enable the evaluation of the hydraulic connectivity in rock masses (Le Borgne et al., 2007). In this context, hydraulic diffusivity is regarded as the key indicator of connectivity between two or more boreholes. Zones

* Corresponding author. Tel.: +81 75 383 3319; fax: +81 75 383 3318.
E-mail addresses: mito@kumst.kyoto-u.ac.jp (Y. Mito), ceashraf@eng.usm.my (M.A.M. Ismail), yamataku@kajima.com (T. Yamamoto).

0022-1694/$ - see front matter © 2011 Elsevier B.V. All rights reserved.
doi:10.1016/j.jhydrol.2011.09.018

with a larger connectivity and diffusivity can act as a preferential flow path and have a substantial impact on the subsurface fluid flow and transport (Becker and Guiltinan, 2010; Black et al., 1986; Black and Kipp, 1981; Hsieh, 1987; Hsieh and Neuman, 1985; Hsieh et al., 1985).

In the past few years, the interpretation of such hydraulic features has been largely improved through advanced hydraulic tests, such as hydraulic tomography (Liu et al., 2002; Yeh and Liu, 2000; Zhu and Yeh, 2005). However, this method is time consuming and computationally intensive because of the inversion required to estimate the spatial distribution of hydraulic properties between the tested holes (Meier et al., 2001). In most cases, the inversion results are strongly influenced by the initial model, the accuracy of which is difficult to assume, especially in three-dimensional cases. In addition, the flow path, which is actually an assembly of several segments or vector-based objects, is often represented as an assembly of grid cells, causing unavoidable errors due to the size and geometry of the grid cells.

In this study, MDS and the IDW transform are implemented for the image processing of hydrogeological structures. These images are derived from the pair-wise hydraulic measurement data set from the cross-hole hydraulic tests. MDS is a set of related statistical techniques and is used here to gain insight in the relations between the pair-wise hydraulic measurement data, as MDS provides a geometrical representation of these relations (Kruskal and Wish, 1978). Meanwhile, IDW, a commonly used interpolation technique, is used to perform a spatial interpolation of the point-wise data generated with MDS (Shepard, 1964; Wackernagel, 1998).

The MDS and IDW transform is then used to identify, characterize and process an image of the preferential flow path in the rock mass. The reliability and applicability of the method were validated through a series of numerical experiments and verified through in situ experiments.

2. Methodology

The pair-wise hydraulic diffusivity data from cross-hole hydraulic tests are used as the input data. These input data are then processed by MDS and IDW to obtain an image of the preferential flow path. The following sub-sections provide details on the data acquisition and data processing procedures.

2.1. Data acquisition by cross-hole hydraulic testing

The cross-hole hydraulic test is a method to assess the hydraulic behavior between two or more boreholes (Hsieh, 1987; Hsieh et al., 1985; Martinez-Landa and Carrera, 2006). Each borehole is subdivided into several intervals using packers (multi-packer system). During the test, fluid is injected into an interval and the hydraulic head response is recorded at other monitoring intervals.

The injection and monitoring intervals are regarded as the points during data processing. The hydraulic diffusivities (hydraulic conductivity divided by specific storage) between an injection interval and monitoring intervals are determined from the hydraulic head at the injection interval, the temporal change in hydraulic heads at the monitoring intervals, and the distance between the injection interval and the monitoring intervals.

The cross-hole hydraulic test is often carried out using an injection borehole as an injection interval and the remaining boreholes as monitoring intervals. This configuration of data points is applied to geo-tomography in the geophysical field. However, this configuration is not essential for cross-hole hydraulic testing. Monitoring intervals can be set in the injection borehole as well because indirect fluid pressure propagation along the angular flow path is rather common, whereas elastic waves propagate in an almost straight line.

To perform a detailed analysis, it is desirable to obtain a matrix of hydraulic diffusivities between all pairs of test intervals by setting monitoring intervals in both the monitoring and the injection boreholes in the cross-hole hydraulic test. A matrix of the hydraulic diffusivities between all test intervals, which were based on the scheme of the cross-hole hydraulic test shown in Fig. 1, is illustrated in Table 1. The fluid injection pressure in the cross-hole hydraulic test is normally specified as a constant by the constant pressure injection test or sinusoidal by sinusoidal pressure test.

2.1.1. Constant pressure injection test

In the constant pressure injection test, the injection and monitoring intervals are treated as a pair of points. The head response in the monitoring intervals as a result of the constant pressure injection in the injection intervals can be obtained through graphical interpretation of the test results by conventional curve matching (Hsieh, 1987; Hsieh and Neuman, 1985; Hsieh et al., 1985).

Labeling the distance between the injection point and the monitoring point as R, the solution for the injection point and monitoring point can be written as (Hsieh and Neuman, 1985):

$$\Delta h = \frac{Q[K_d]^{1/2}}{4\pi R D^{1/2}} erfc\left[\left(\frac{R^2 S_s}{4K_d t}\right)^{1/2}\right] \quad (1)$$

$$D = \begin{vmatrix} K_{11} & K_{12} \\ K_{21} & K_{22} \end{vmatrix}, \quad (2)$$

where Δh is the head increase at the monitoring point, Q is the volumetric injection rate at the injection point, t is time elapsed, S_s is the specific storage of the rock mass, D is the determinant of K as expressed in (2) and K_d is the directional hydraulic conductivity between the injection and monitoring intervals.

The dimensionless form of (1) is expressed as:

$$\Delta h_{PD} = erfc[1/4(t_D)^{1/2}], \quad (3)$$

where Δh_{PD} is the change in the dimensionless hydraulic head and t_D is the dimensionless time, which are, respectively, defined as:

$$\Delta h_{PD} = (4\pi R \Delta h/Q)[D/K_d]^{1/2}, \quad (4)$$

and

$$t_D = K_d t/(R^2 S_s). \quad (5)$$

To analyze the constant pressure injection test results, a theoretical type curve of Δh_{PD} versus t_D was prepared on a log–log plot according to (4) and (5).

Then the following steps are performed for each monitoring interval j:

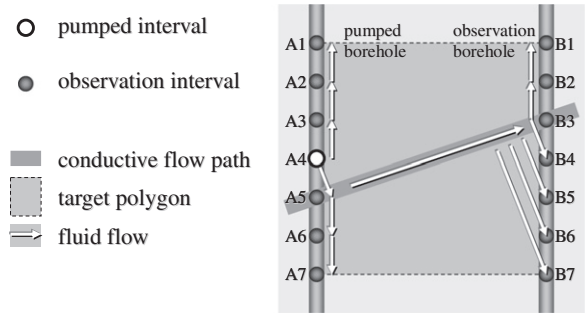

Fig. 1. Schematic of cross-hole hydraulic test with the superconductive flow path.

Table 1
An illustration of a matrix of hydraulic diffusivities between all the test intervals (unit: $\times 10^{-4}$ cm^2/s).

	A1	A2	A3	A4	A5	A6	A7	B1	B2	B3	B4	B5	B6	B7
A1	0													
A2	229	0												
A3	63	229	0											
A4	13	24	63	0										
A5	9	13	24	63	0									
A6	7	9	13	24	229	0								
A7	5	7	9	13	63	229	0							
B1	5	7	7	8	7	5	5	0						
B2	7	7	9	13	9	7	5	229	0					
B3	7	9	17	33	17	9	7	63	229	0				
B4	9	13	33	46	33	13	9	13	24	63	0			
B5	7	9	17	33	17	9	7	9	13	24	29	0		
B6	5	7	9	13	9	7	7	7	9	13	24	29	0	
B7	5	5	7	9	7	7	5	5	7	9	13	63	229	0

(i) Plot Δh_j versus t on a log–log plot with log cycles of the same size as the type curve.
(ii) Superimpose the data on the type curve by keeping the coordinate axes of the two plots parallel to obtain the best fit between the in situ test data and the theoretical type curve (Fig. 2).
(iii) Choose an arbitrary match point anywhere on the overlapping portion of the two log–log graphs and denote the corresponding values of Δh_j, Δh_{PD}, t and t_D by Δh_j^*, Δh_{PD}^*, t^* and t_D^* (Fig. 2).

Substitute the above quantities into (4) and (5) to compute:

$$D/K_d = (Q_j \Delta h_{PD}^* / 4\pi R_j \Delta h_j^*)^2, \tag{6}$$

where D is the determinant of K_d, and the directional diffusivity is expressed by:

$$K_d/S_s = R_j t_D^*/t^*. \tag{7}$$

By matching the measured head response to the type curve on the log–log plot, the directional hydraulic diffusivity K_d/S_s can be computed from the constant pressure injection test. An example of the hydraulic diffusivity configuration computed from the constant pressure injection test is shown in Table 1.

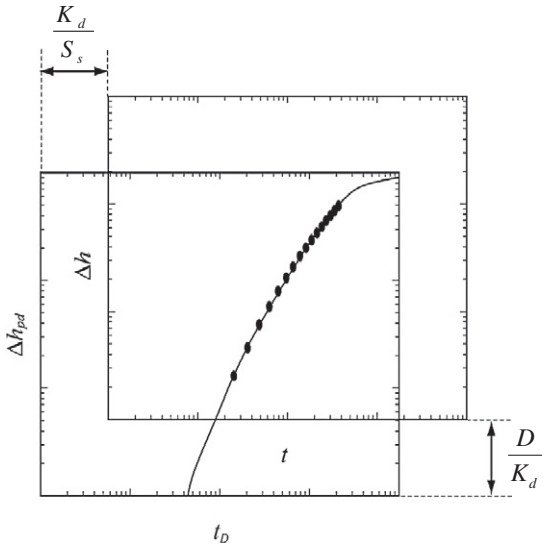

Fig. 2. Log–log plot of the measured head respond versus time with superimposed and fitted type curves.

2.1.2. Sinusoidal pressure test

The sinusoidal pressure test is a cross-hole technique in which a small zone of one borehole is subjected to a sinusoidal variation of pressure while a similar zone in an adjacent borehole is monitored (Black and Kipp, 1981). The pressure variation in the source zone is created by careful injection and abstraction. This sinusoidally varying pressure is detected in the receiver zone. The amplitude of the pressure variation is smaller in the receiver zone than in the source zone because the pressure waves require some time to diffuse from the source to the receiver. The decrease in amplitude and the phase lag of the received signal compared to the source signal depend on the geometry and hydrogeological properties of the flow paths, which can indirectly be employed to compute the hydraulic diffusivity of the rock mass (Barker, 1988; Black et al., 1986; Black and Kipp, 1981; Motojima et al., 1993).

The ratio of the amplitude attenuation $|G^*|/|G_0^*|$ of the sinusoidal pressure and the time lag of the phase (phase lag) Φ^* can be obtained by the following equations (Black and Kipp, 1981):

Amplitude attenuation,

$$\frac{|G^*|}{|G_0^*|} = \frac{N_0\left[r\left(\frac{\omega}{\kappa}\right)^{1/2}\right]}{N_0\left[r_0\left(\frac{\omega}{\kappa}\right)^{1/2}\right]}, \quad \text{and} \tag{8}$$

Phase lag,

$$\Phi^* = \Phi_0\left[r\left(\frac{\omega}{\kappa}\right)^{1/2}\right], \tag{9}$$

where N_0 is the amplitude of the Kelvin function, r is the distance from the point or line source, r_0 is the radius of sphere or cylinder enveloping the source, ω is the frequency of the periodic functions and κ is the hydraulic diffusivity.

The hydraulic diffusivity κ can be obtained by measuring the amplitude attenuation $|G^*|/|G_0^*|$ or the phase shift Φ^*. The sinusoidal pressure test thus allows estimation of the hydraulic diffusivity without measuring the flow rate during a testing period. Moreover, the resulting diffusivity values are not influenced by either the initial groundwater pressure or any changes. This test can be used for estimating the three-dimensional hydraulic continuity of joints and cracks. To this end, the pressure-receiving boreholes must be placed in the three-dimensional region around the source borehole (Motojima et al., 1993). The equipment required for performing the sinusoidal pressure tests is well described by Holmes, 1984; Holmes and Sehlstedt, 1985 and Motojima et al., 1993.

2.2. Hydraulic configuration of the test intervals

The configuration of the test intervals in a cross-hole hydraulic test can be expressed by Cartesian coordinates, which represent

Table 2
Matrix of the hydraulic distance, which is obtained from the matrix of hydraulic diffusivities as shown in Table 1 (unit: s/cm).

	A1	A2	A3	A4	A5	A6	A7	B1	B2	B3	B4	B5	B6	B7
A1	0													
A2	44	0												
A3	158	44	0											
A4	794	417	158	0										
A5	1096	794	417	158	0									
A6	1514	1096	794	417	44	0								
A7	2069	1514	1096	794	158	2069	0							
B1	2069	1514	1514	1096	1514	1514	2069	0						
B2	1514	1514	1096	794	1096	1096	2069	44	0					
B3	1514	1096	575	302	575	794	1514	158	158	0				
B4	1096	794	302	575	302	1096	1096	794	794	158	0			
B5	1514	1096	575	302	575	1514	1514	1096	1096	417	158	0		
B6	2069	1514	1096	794	1096	1514	1514	1514	1514	794	417	44	0	
B7	2069	2069	1514	1096	1514	2069	2069	2069	2069	1096	794	158	44	0

the distances between the intervals in the real geographical space. In our study, the configuration of test intervals is also expressed in an alternative coordinate system: in this case, the coordinates do not represent geographical distances but hydraulic distances, which are proportional to the travel time of water over this distance. These hydraulic coordinates can be considered inside an imaginary hydraulic subspace, where the hydraulic distance is measured.

The reciprocal of hydraulic diffusivity is a variable appropriate to represent the hydraulic distance, just as "slowness" is the reciprocal of velocity in the tomography case. The hydraulic distance D_h is defined as the time elapsed for the hydraulic diffusion K/S_s to occur per unit distance l (length) and can be expressed by:

$$D_h = \left(\frac{K/S_s}{l}\right)^{-1}. \tag{10}$$

A matrix of the hydraulic distance, as shown in Table 2, can be obtained from the matrix of the hydraulic diffusivities between the pairs of test intervals shown in Table 1.

2.2.1. Multidimensional scaling

MDS was used in this study to express the configuration of the hydraulic distance between test intervals (Table 2) as coordinates in an imaginary hydraulic subspace.

MDS is a mathematical procedure by which information contained in a data set can be represented by points in a space. Essentially, the purpose of the MDS is to provide a visual representation of the pattern of proximities (i.e., similarities or distances) among a set of objects.

MDS plots objects on a map such that objects that are very similar to each other are placed near each other on the map and objects that are very different from each other are placed far away from each other on the map (Kruskal and Wish, 1978; Naugpal, 2001).

The main output of MDS is a spatial representation of a geometric configuration of points on a map. Each point in the configuration corresponds to one object. The configuration on the map can reveal the hidden structure of the data and make the data much easier to comprehend.

MDS can also be used indirectly to analyze data that are not real proximities but that can nevertheless be expressed as proximities. The hydraulic distance that was computed from the hydraulic diffusivities obtained from the cross-hole hydraulic test can therefore be considered an expression of proximity.

Several algorithms to determine a configuration of a set of objects have been suggested in MDS. Kruskal's algorithm (Kruskal and Wish, 1978), which is widely applied, is adopted in this study.

In MDS, each object is represented by a point, where x_i is used to indicate the point that corresponds to the ith object. X is used to indicate the entire configuration of points from $x_i \ldots\ldots x_l$. In this kind of configuration, the distance between the points of X plays a central role. The distance between two points x_i and x_j is indicated by:

$$d_{ij} = d(x_i, x_j), \tag{11}$$

where d_{ij} is the distance from x_i to x_j.

Not all proximities between all pairs of data d_{ij} must be known to obtain the hydraulic configuration, because MDS is a statistical method that is able to estimate missing proximity values. This feature is of practical significance because actual field data sets often suffer from missing observations.

With the MDS method, a configuration of data points in the hydraulic subspace can be obtained from the matrix of hydraulic distances (Table 2), as shown in Fig. 3. Although it is quite difficult to imagine the fundamental structure of the flow path from the matrix of hydraulic diffusivities in Table 1 and the hydraulic distances in Table 2, the graphical expression from the MDS in Fig. 3 gives insight into all hydraulic relationships between and among the points (in the cross-hole hydraulic test) and the approximated hydro-geological structure. For example, the existence of principal pathways between A5 and B3 can be inferred at a glance in Fig. 3.

2.3. Geographical configuration of equally spaced obstacle points in the hydraulic subspace

In the hydraulic subspace, the hydraulic diffusivity is constant. This way, "obstacles" for fluid flow (like clay particles in soil), which are represented in the hydraulic subspace by a set of equally

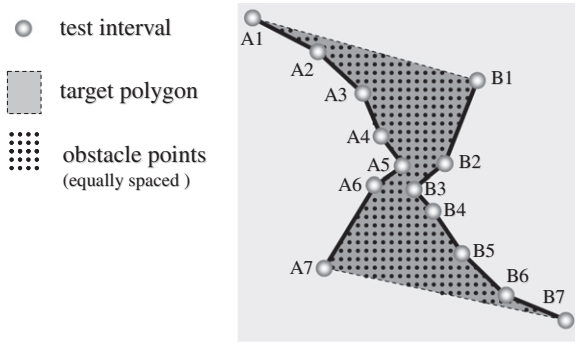

Fig. 3. Hydraulic configuration of data points and equally spaced obstacle points in the hydraulic subspace.

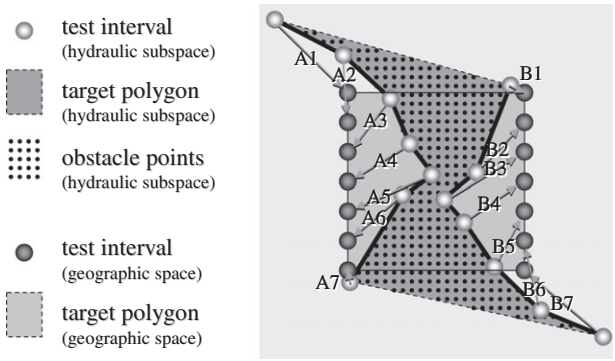

Fig. 4. Hydraulic and geographical configurations of data points in the geometric hyperspace.

spaced points, can easily be detected. What needs to be done now is to relocate these obstacles in the original geographical space, so that we can locate the obstacles in the real world.

Therefore, we need to refer to the relationship between the geographical and hydraulic configurations of data points, which is assumed as follows (see Fig. 4).

The transformation between two spaces is implemented in an imaginary geometric hyperspace, where the dimensionless geometric distance is measured. The relative configuration of points in this imaginary geometric hyperspace is identical with the relative configurations of the corresponding points in the geographical and in the hydraulic space.

The area (volume) of the target polygon (polyhedron), which is surrounded by data points, is the same in the three considered spaces (geographical, hydraulic and imaginary geometric).

The configuration of the target polygons in the geometric hyperspace is determined such that the barycenters of the target polygons (polyhedrons) are identical in the three spaces (geographical, hydraulic, and imaginary geometric) and such that the three representations of a given data point are as aligned as possible.

With these assumptions, the configuration of a set of equally spaced points in the geographical space can be determined by spatial interpolation using IDW in the geometric hyperspace.

2.3.1. Inverse distance weighting

The IDW method is the simplest and most widely used spatial interpolator based on the spatial correlation between scattered points (Shepard, 1964; Wackernagel, 1998). IDW estimates the value at any unsampled site by weighting the available data samples by a power of p, the inverse distance between the sampled location and the unsampled location (scaling the weights to be a unit sum). In the inverse distance weighted interpolation, the interpolation value of $Z(x')$ in the position x' is calculated based on the following expression:

$$Z(x') = \sum_{i=1}^{n} w_i Z(x_i), \tag{12}$$

where n is the number of scatter points (data samples) in the set, $Z(x_i)$ are the values at the sampled points (e.g., the data values set), and w_i are the weights assigned to each sampled point. This weight is calculated with the following function:

$$w_i = \frac{h_i^{-p}}{\sum_{j=1}^{n} h_j^{-p}}, \tag{13}$$

where p is a positive real number called the power parameter (typically, $p = 2$) and h_i is the distance from the sampled location to the unsampled location for which an interpolated value is sought.

The weight function varies from a value of unity at the sampled site to a value approaching zero at an infinite distance of the sampled location, so that samples lying closer to the unsampled site receive a higher weight. The weight function is normalized such that the weights sum to unity. The vector from a point in the hydraulic space to the corresponding point in the geographical space is given by a linear combination of the vectors linking the locations of the sampled sites in the hydraulic space to their corresponding geographical locations. A configuration of a set of equally spaced points in the geographical space can be obtained from the configurations, as shown in Fig. 5.

2.4. Visualization of the flow path

The spatial density of obstacle points in the geographical space is considered to represent the degree of impermeability of the rock. Therefore, regions with a lower density of obstacle points correspond to preferential flow paths.

From the results of the preliminary parametric study (see Section 3), the relationship between the density of obstacle points and hydraulic diffusivity was clarified. This relationship enables the estimation of the hydraulic diffusivity at an arbitrary location within the target polygon in the geographical space. If the specific storage capacity of the rock is known, the spatial distribution of the hydraulic conductivity can be found.

Several kinds of methods can be considered to measure and display the spatial density of the points. For instance, it can be assessed as the number of obstacles per cell of a superimposed raster (Fig. 6). Another approach consists of counting the number of obstacles within a circular neighborhood, which results in a continuous spatial density distribution.

2.5. Three-dimensional model

The proposed two-dimensional methodology can easily be applied to the three-dimensional context, which involves the three-dimensional geographical space, hydraulic subspace and geometric

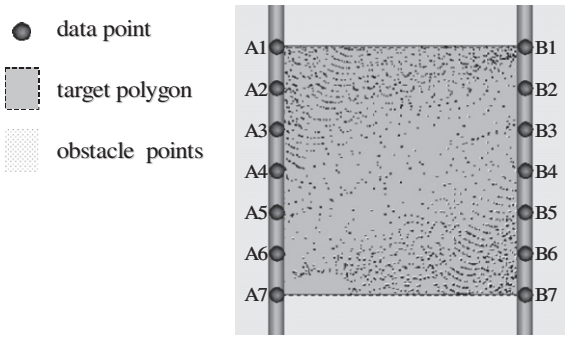

Fig. 5. Geographical configuration of obstacles points in the geographical space.

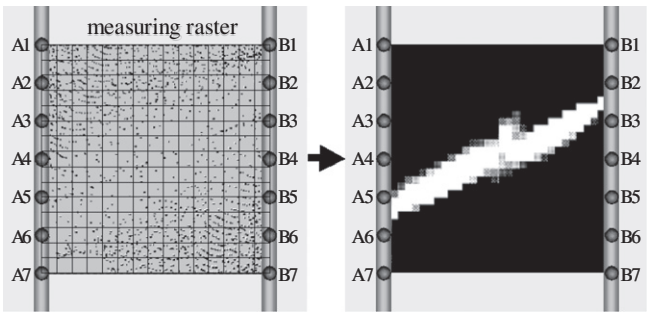

Fig. 6. Raster-base measurement and expression technique.

hyperspace. In the three-dimensional cases, the target polygon in the two-dimensional cases is generalized as the target polyhedron.

Because both MDS and IDW are intrinsically multidimensional methods, the three-dimensional space continua in the form of a polyhedron can be transformed in a similar way as the two-dimensional one. The hydraulic properties can be evaluated from the volumetric spatial density of obstacle points in the geographical space. Fig. 7 shows the scheme of the three-dimensional method.

3. Verification of the methodology

3.1. Numerical experiments

A series of numerical experiments was conducted to verify the applicability of the proposed method and investigate its performance.

Two-dimensional and three-dimensional continuum models, simulating different positions of a super-conductive flow path with a certain width, were made in a region with a horizontal width of 110 m and a height of 80 m, as shown in Fig. 8. A hydraulic conductivity of 10^{-5} m/s was given to the super-conductive flow path, whereas 10^{-7} m/s was given to the surrounding rocks. A uniform specific storage of 10^{-3} m^{-1} was assumed throughout the model region.

The sides and the top of the region were head-specified boundaries. At the bottom of the region, an impermeable boundary was assumed. The numerical cross-hole test with a constant injection pressure was conducted using seven test intervals with 10-m holes.

The hydraulic diffusivity between each pair of test intervals was determined from the computed temporal changes in the hydraulic

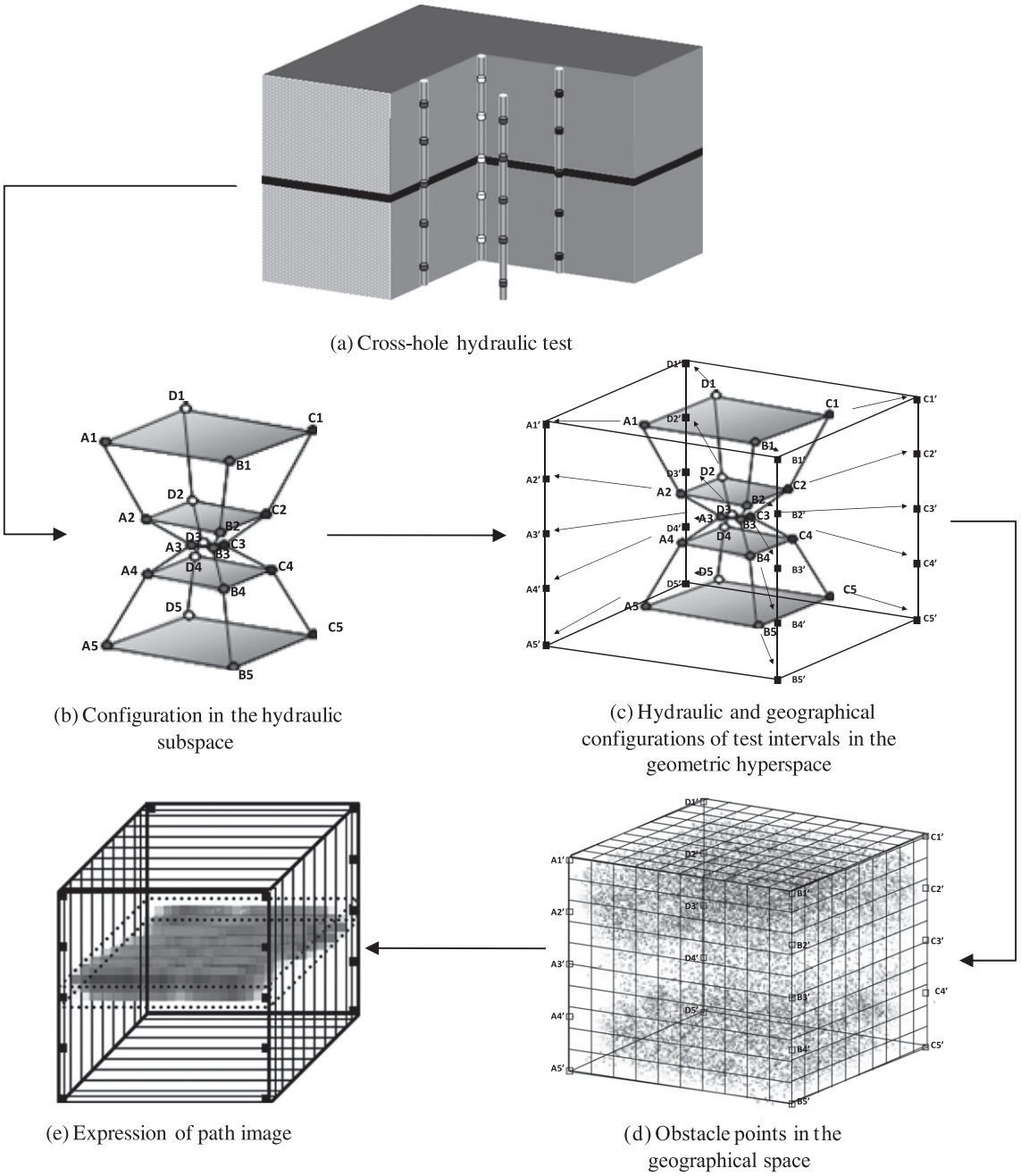

Fig. 7. Schematic for the three-dimensional case procedure.

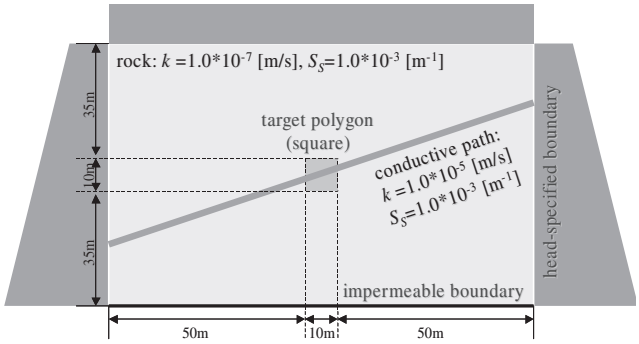

(a) Two-dimensional model

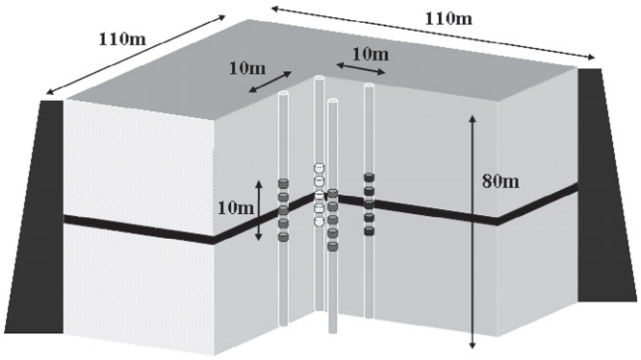

(a) Three-dimensional model

Fig. 8. Two-dimensional and three-dimensional continuum models for finite element analysis of unsteady state groundwater flow with an example of a conductive flow path.

head, which were obtained from the finite element analysis of the unsteady state groundwater flow.

The hydraulic configuration of test intervals was determined by MDS using hydraulic distances between all pairs of test intervals. Sequentially, the configuration of obstacles was determined by IDW, and then the image of the flow path was obtained by counting the number of obstacles per cell of the raster, as shown in Fig. 8.

Fig. 9 shows several sets of the original hydrogeological structure, the hydraulic configuration of data points and the computed flow path image in a case of a horizontal flow path intersecting the target polygon at several depths. The pixels with a lower density (higher hydraulic conductivity) were drawn with a lighter gray in the computed image.

The horizontal line-shaped flow path emerged at the appropriate position. In addition, the hydraulic configuration gave not only the hydraulic relationship between (and/or among) data points but also an integrated interpretation of the test results in light of the actual phenomena.

Figs. 10 and 11 show cases where an oblique conductive path intersects the target polygon. Although Fig. 9 shows that the method can be applied successfully for horizontal flow paths, there are some differences in performance in the cases of oblique and vertical conductive paths (Figs. 10 and 11). The preferential flow path in the second example in Fig. 11 is less accurately reproduced compared to the other examples: the zone visualized as conductive flow path not only contains the path but also includes a substantial part of its surroundings. Meanwhile, the vertical flow paths shown in Fig. 12 cannot be visualized at all. Nevertheless, the computed pattern of hydraulic configuration data points and equally spaced obstacle points shown in Fig. 12b hints at the presence of a preferential flow path.

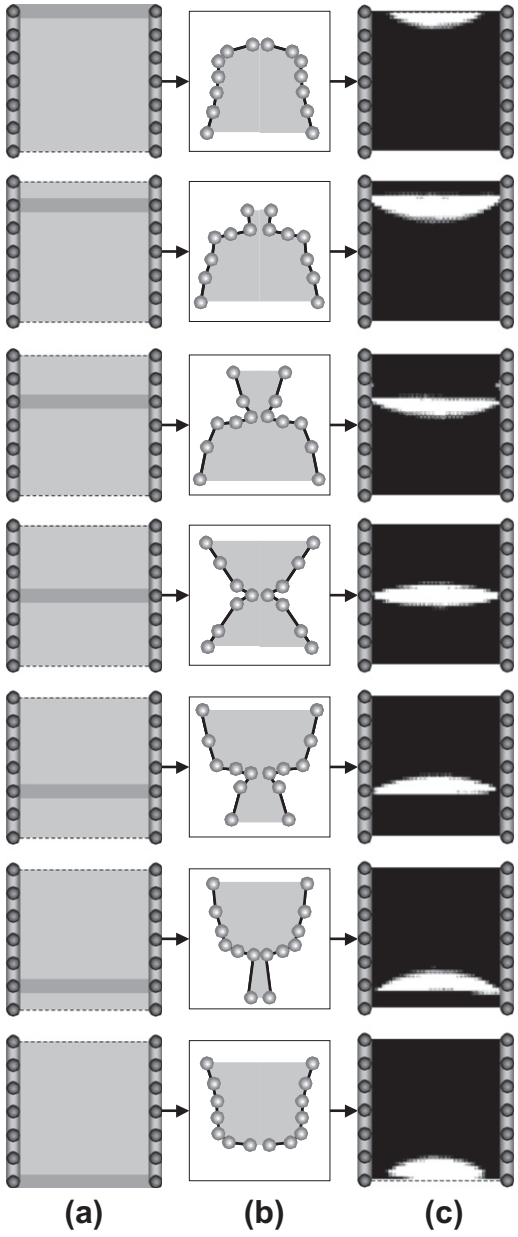

Fig. 9. Comparisons between the original hydro-geological structure (a) and the computed imaging result (c) in the cases where a horizontal conductive path intersects the target polygon at several depths. The pixels with lower density are drawn with a lighter gray in the computed image. The hydraulic configuration of data points (b) is also shown.

Fig. 13 shows how the presence of multiple flow paths is visualized. This is important for the evaluation of the hydraulic behavior of a real fracture system because such a system often contains multiple flow paths. As for the horizontal and the oblique fracture patterns, appropriate images were also obtained in this case. The image of the multiple flow paths can be used not only to assess the physical connections but also to gain insight into the hydraulic connections between individual fractures, which influence the fluid flow.

Three-dimensional models are important for constructing a fracture network model that is accurate to the real structures. Fig. 14 shows several original hydrogeological structures, the hydraulic configurations of data points corresponding with these structures and the computed flow path images. The original hydrogeological structures represent cases where a horizontal flow path

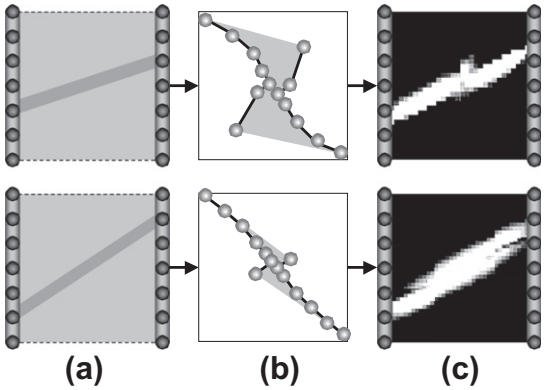

Fig. 10. The same comparison as shown in Fig. 9 in cases where an oblique conductive path intersects both sides of the target polygon.

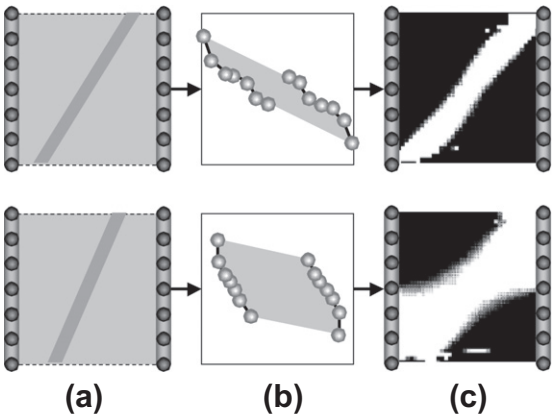

Fig. 11. The same comparison as in Fig. 9 in the case where an oblique conductive path intersects both the top and the bottom of the target polygon.

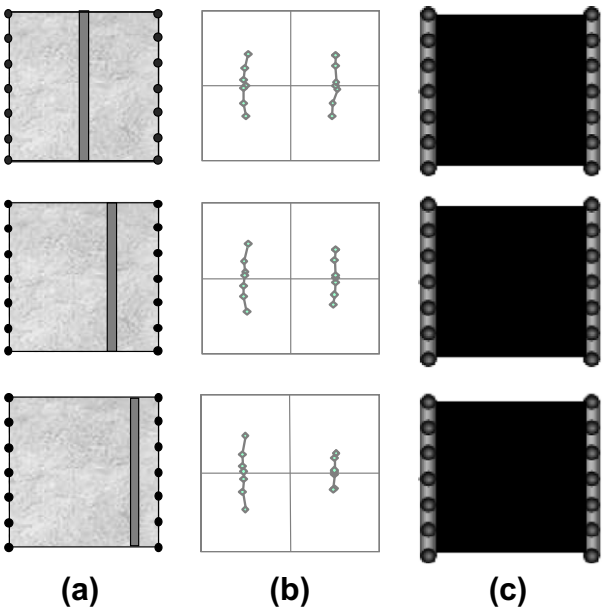

Fig. 12. The same comparison as in Fig. 9 in the case where a vertical conductive path intersects both the top and bottom of the target polygon.

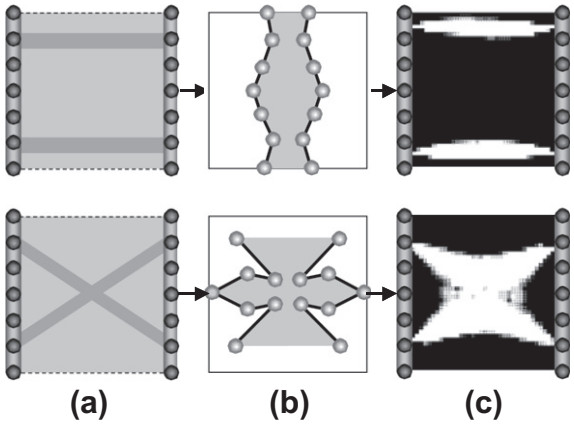

Fig. 13. The same comparison as in Fig. 9 in the case where two conductive paths intersect the target polygon.

intersects the target polygon at different depths, similar to the case of the two-dimensional models shown in Fig. 9. Fig. 15 shows the results obtained for oblique conductive paths intersecting both sides of the target polygon. In the computed images, the lighter gray colors indicate zones with a higher hydraulic conductivity. Because the images obtained by the two-dimensional and three-dimensional numerical experiments show the assumed flow path at the appropriate location, it can be assumed that the proposed imaging method is reliable.

4. Applicability of the methodology

4.1. In situ experiments

The applicability of the imaging method, which shows good performance in the numerical experiments, was also examined by field experiments at two sites using two-dimensional and three-dimensional models.

4.1.1. Field experiment in tertiary sedimentary rocks – two-dimensional case

A cross-hole hydraulic test with constant injection pressure as explained in Section 2.1.1 was conducted using two boreholes, which were drilled in a tertiary alternation of mudstone, sandstone and pumice tuff with a homoclinal structure.

The geographical configuration of the nine test intervals and the imaging results given by the proposed method were drawn on the underlying geological profile, as shown in Fig. 16. The objective polygon contains mudstone, pumice tuff layers and sandstone sub-layers I–III.

The image of the hydrogeological structure is composed of several layers with different hydraulic properties. The direction of these layers corresponds with the underlying geological structure. Furthermore, the sandstone layer II and the pumice tuff layers, where joints are denser show a higher permeability compared to the other geological layers. Moreover, in zones with mudstone and sandstones I and III, where the joints are more sparse, a lower permeability is indicated. This means that the proposed method provides an appropriate two-dimensional image of the hydrogeological structure of the rock mass in this particular case.

4.1.2. Field experiment in cretaceous sedimentary rocks – three-dimensional case

The cross-hole hydraulic test with sinusoidal pressure, as explained in Section 2.1.2, was conducted using three boreholes, which were drilled in a cretaceous alternation of sandstone and

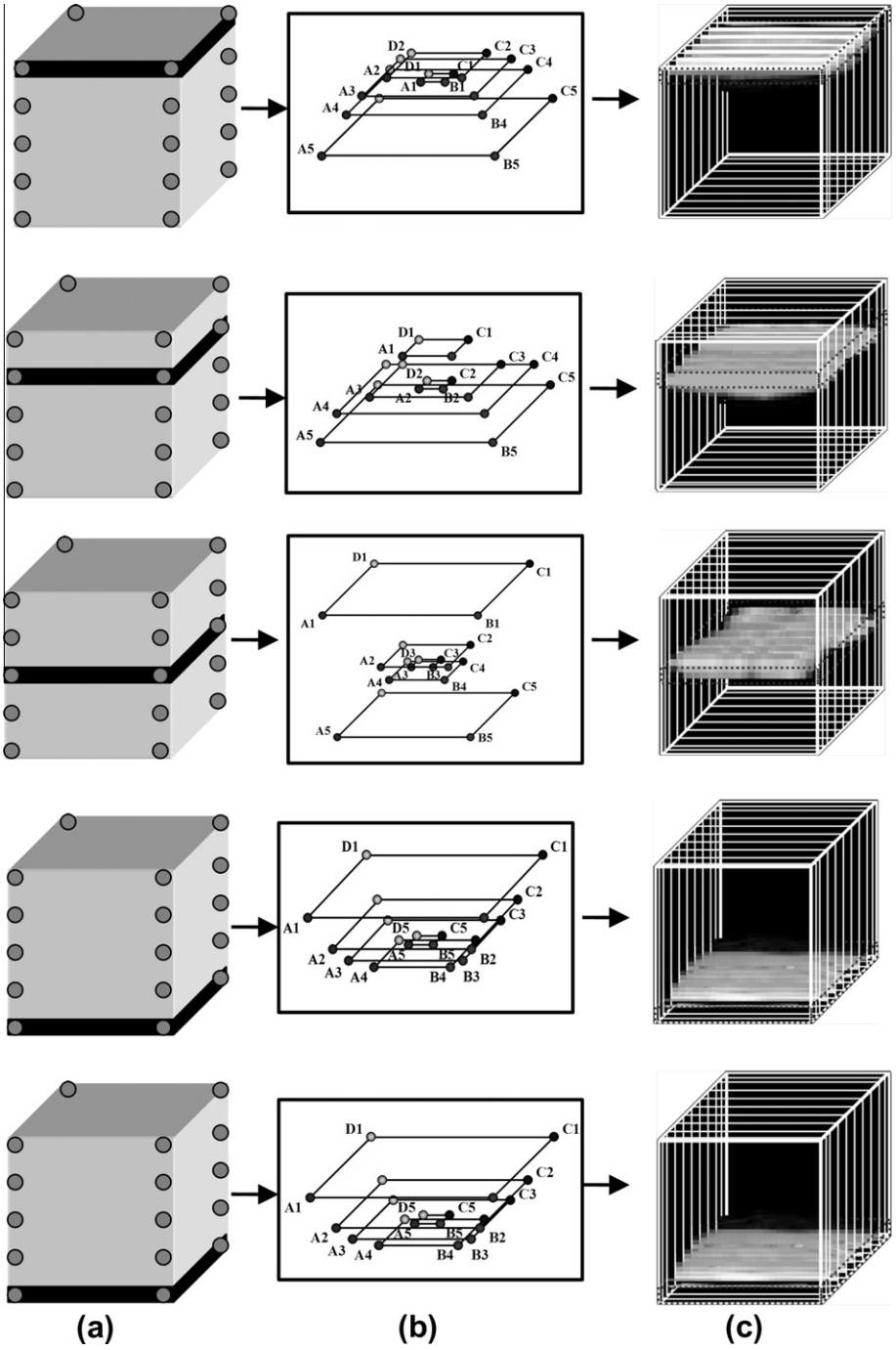

Fig. 14. Comparisons between the original hydro-geological structure in three dimensions (a) and the computed imaging result (c) in the case where a horizontal conductive path intersects the target polygon at several depths. The pixels with lower density are drawn with a lighter gray in the computed image. The hydraulic configuration of data points (b) is also shown.

mudstone. Fig. 17a shows the geographical configuration of the eleven source and observation intervals, which were set at a depth of 25–35 m from the exploration adit of the underground power station construction site. The presence of a steep fracture zone in the target polyhedron is confirmed by both the adit wall observation and the borehole television (BTV) observation (Fig. 17a), although this fracture zone does not directly appear at any source or observation interval. Fig. 17b shows the hydraulic configuration of the data points. Fig. 17c shows the computed image of the preferential flow path. This image shows good agreement with the fracture zone, which is the only hydrogeological structure in the target polyhedron that can be a super conductive flow path. This means that the proposed methodology is able to deliver a reliable three-dimensional image for this field test.

5. Discussion and conclusion

Preferential flow paths are ubiquitous and always play an important role in the hydraulic behavior of a rock mass. The influence of these flow paths on the hydraulic behavior of a rock mass is difficult to characterize due to the inherent complexities in

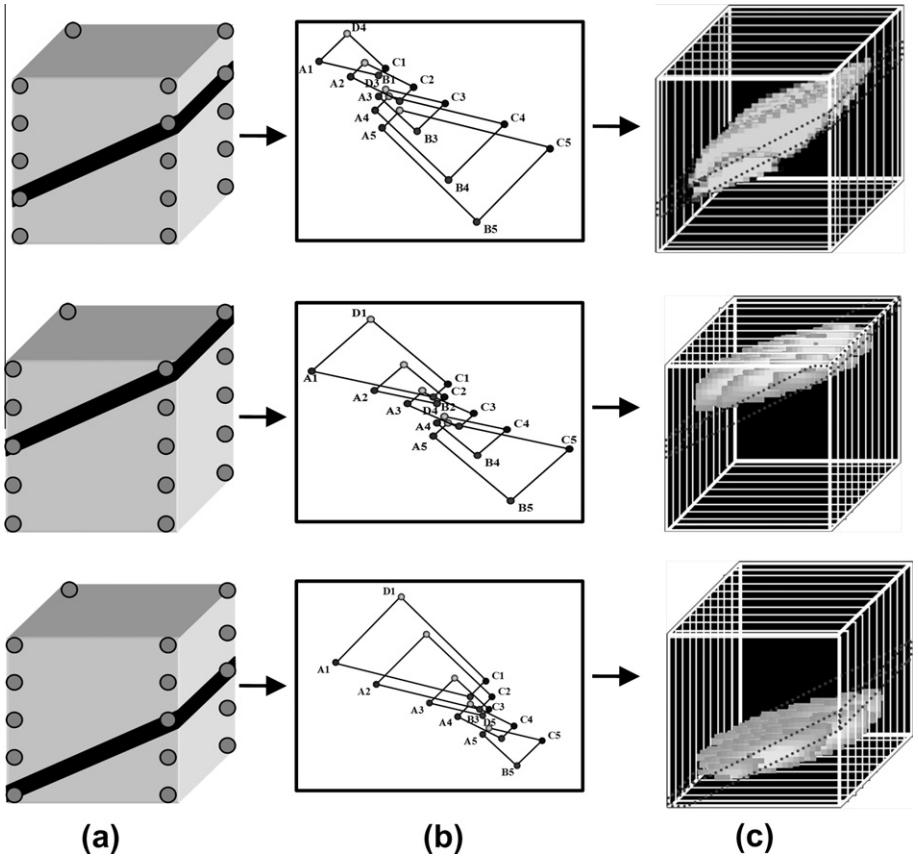

Fig. 15. The same comparison as in Fig. 14 in the cases where an oblique conductive path intersects both sides of the target polyhedron in the three-dimensional cases.

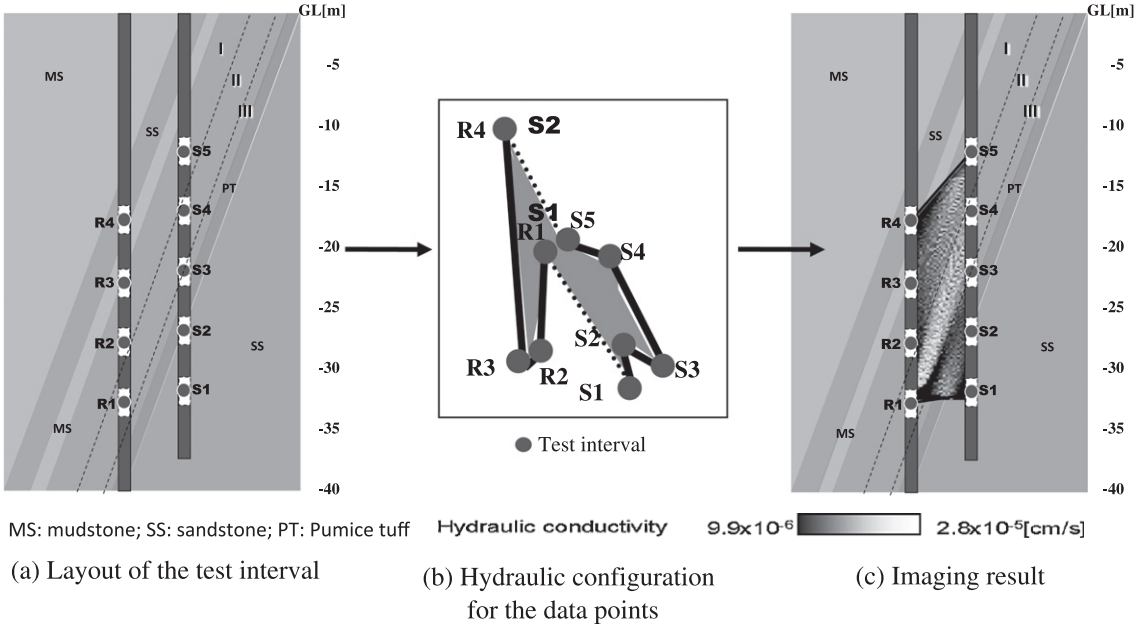

Fig. 16. Layout of the test intervals and the imaging result on a geological map for the two-dimensional case. The sandstone layer that is located in the mid of the objective polygon can be subdivided into three sub-layers (I–III) from the point of view of rock properties.

fracture network geometries, densities and connectivity. These factors often dominate the selection of the methodology used for the detection, characterization and visualization of flow paths.

In this study, a new method for visualizing the hydrogeological structure in rock masses that is simpler than computationally intensive inference or inversion was developed. The method was validated by numerical and in situ experiments. It does not require any kind of initial model and is able to determine the geometric and hydraulic properties of the flow paths, such as orientation, shape and hydraulic conductivity, in both two and three dimensions.

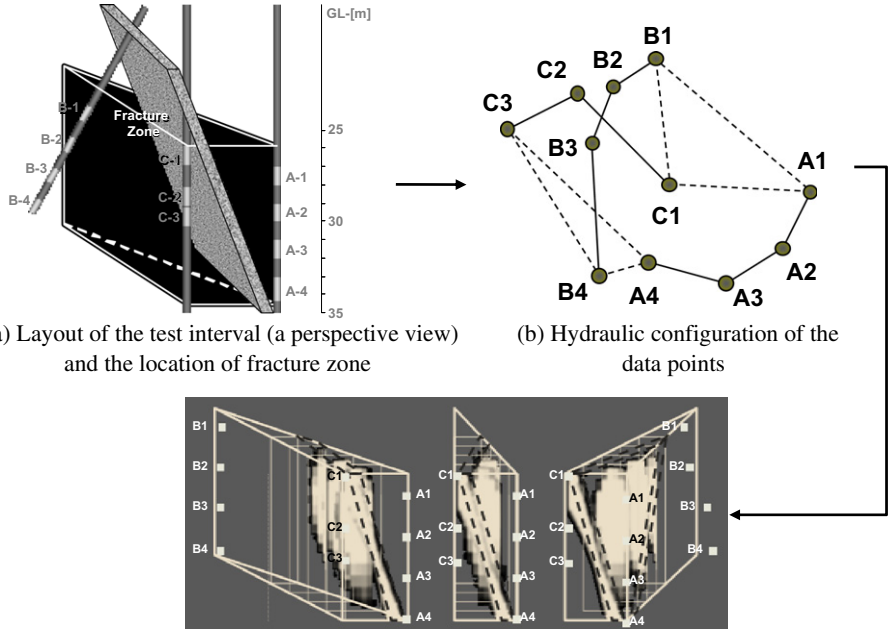

(a) Layout of the test interval (a perspective view) and the location of fracture zone

(b) Hydraulic configuration of the data points

(c) Three dimensional image of the preferential flow path (perspective views in the three different directions)

Fig. 17. Layout of the test interval and the image of the preferential flow path for the three-dimensional case. The fracture zone as inferred in (a) is strongly associated with the image obtained in (c).

Although the method can be applied successfully, there are some differences in performance between the various situations presented in this study. The method appears to perform well for detecting the preferential flow path if there is a difference in hydraulic diffusivity between the point pairs involved in the cross-hole test. From the numerical analysis results, it was found that the degree of intersection determines whether the preferential path will have a large or a small impact on the measured diffusivity. The higher the degree of intersection (i.e., in the case of a horizontal flow path), the larger the impact on the measured hydraulic diffusivity will be. In case of such a high degree of intersection, the preferential flow path can be clearly visualized. However, if the degree of intersection is smaller (i.e., an oblique flow path) or similar for all point pairs, as in the vertical flow path cases, the calculated diffusivity for all pairs will be similar, and thus the preferential flow path cannot be visualized.

The possible orientation of the preferential flow path needs to be estimated before the methodology developed in this study can be applied. The identification of the preferential flow path orientation by means of geological mapping or geophysical techniques gives the information required to determine the orientation of the boreholes for the cross-hole test, so that the preferential flow path can be detected. In case of a dominant vertical flow path in the study area, inclined boreholes that can intercept the vertical flow path must be included in the cross-hole test.

Acknowledgments

The authors are most grateful to the Kajima Corporation for their assistance with the assessment of the in situ experiments and to other persons for providing invaluable input for this paper.

References

Barker, J.A., 1988. A generalized radial flow model for hydraulic tests in fractured rock. Water Resour. Res. 24 (10), 1796–1804.

Becker, M.W., Guiltinan, E., 2010. Cross-hole periodic hydraulic testing of inter well connectivity. In: Thirty-fifth Workshop on Geothermal Reservoir Engineering, Stanford University.

Black, J.H., 1978. Use of slug test in groundwater investigations. Water Serv. 82 (985), 174–178.

Black, J.H., Kipp, K.L., 1981. Determination of hydrogeological parameters using sinusoidal pressure tests – a theoretical appraisal. Water Resour. Res. 17 (3), 686–692.

Black, J.H., Barker, J.A., Noy, D.J., 1986. Crosshole Investigations – the Method Theory and Analysis of Crosshole Sinusoidal Pressure Tests in Fissured Rock, Stripa Project IR 86-03, SKB, Stockholm.

Bonin, B., Colin, M., Dutfoy, A., 2000. Pressure building during the early stages of gas production in a radioactive waste repository. J. Nucl. Mater. 281 (1), 1–14.

Le Borgne, T. et al., 2007. Comparison of alternative methodologies for identifying and characterizing preferential flow paths in heterogeneous aquifers. J. Hydrol. 345 (3–4), 134–148.

Bouwer, H., Rice, R.C., 1976. A slug test method for determining hydraulic conductivity of unconfined aquifers with completely or partially penetrating wells. Water Resour. Res. 12 (3), 423–428.

Butler, J.J., Zhan, X.Y., 2004. Hydraulic tests in highly permeable aquifers. Water Resour. Res. 40 (12).

Cassiani, G., Bohm, G., Vesnaver, A., Nicolich, R., 1998. A geostatistical framework for incorporating seismic tomography auxiliary data into hydraulic conductivity. J. Hydrol. 206 (1–2), 58–74.

Chung, I.M., Cho, W.C., Heo, J.H., 2003. Stochastic hydraulic safety factor for gas containment in underground storage caverns. J. Hydrol. 284 (1–4), 77–91.

Giramonti, A.J., Lessard, R.D., Blecher, W.A., Smith, E.B., 1978. Conceptual design of compressed air energy-storage electric-power systems. Appl. Energy 4 (4), 231–249.

Holmes, D.C., 1984. Crosshole Investigations – Equipment Design Considerations for Sinusoidal Pressure Tests, Stripa Project IR 84-05, SKB, Stockholm.

Holmes, D.C., Sehlstedt, M., 1985. Crosshole investigations – design of the hydraulic testing system. In: Symposium on in-situ Experiments in Granite Associated with the Disposal of Radioactive Waste. OECD Nuclear Energy Agency and SKBF, Stockholm, pp. 203–213.

Houlsby, A.C., 1976. Routine Interpretation of the lugeon water test. Quart. J. Eng. Geol. Hydro-Geol. 9 (4), 303–313.

Hsieh, P.A., 1987. Characterizing the hydraulic properties of fractured rock masses methodology and case studies. In: The 28th US Symposium on Rock Mechanics (USRMS). A. A. Balkema, Tucsan, AZ, pp. 465–472.

Hsieh, P.A., Neuman, S.P., 1985. Field determination of the 3-dimensional hydraulic conductivity tensor of anisotropic media 1. Theory. Water Resour. Res. 21 (11), 1655–1665.

Hsieh, P.A., Neuman, S.P., Stiles, G.K., Simpson, E.S., 1985. Field determination of the 3-dimensional hydraulic conductivity tensor of anisotropic media 2. Methodology and application to fractured rocks. Water Resour. Res. 21 (11), 1667–1676.

Kipp, K.L., 1985. Type curve analysis of inertial effects in the response of a well to a slug test. Water Resour. Res. 21 (9), 1397–1408.
Kiyoyama, S., 1990. The present state of underground crude oil storage technology in Japan. Tunn. Undergr. Space Technol. 5 (4), 343–349.
Kjorholt, H., Broch, E., 1992. The water curtain – a successful means of preventing gas leakage from high-pressure unlined rock caverns. Tunn. Undergr. Spae Technol. 7 (2), 127–132.
Kruskal, J.B., Wish, M., 1978. Multidimensional Scaling. Quantitative Applications in the Social Sciences. SAGE Publication, London.
Lindblom, U., 1989. The performance of water curtains surrounding rock caverns used for gas-storage. Int. J. Rock Mech. Min. Sci. Geomech. Abstr. 26 (1), 85–97.
Liu, S.Y., Yeh, T.C.J., Gardiner, R., 2002. Effectiveness of hydraulic tomography: sandbox experiments. Water Resour. Res. 38 (4).
Martinez-Landa, L., Carrera, J., 2006. A methodology to interpret cross-hole tests in a granite block. J. Hydrol. 325 (1–4), 222–240.
Meier, P.M., Medina, A., Carrera, J., 2001. Geostatistical inversion of cross-hole pumping tests for identifying preferential flow channels within a shear zone. Ground Water 39 (1), 10–17.
Motojima, I., Kono, I., Nishigaki, M., 1993. Crosshole permeability testing method in bedrock. Soils Found. 33 (4), 108–120.
Naugpal, P.S., 2001. Guide to Advanced Data Analysis: Using IDAMS Software. UNESCO, Division of Information and Informatics.
Park, B.Y. et al., 2002. Determination of the hydraulic conductivity components using a three-dimensional fracture network model in volcanic rock. Eng. Geol. 66 (1–2), 127–141.
Pickens, J.F., Grisak, G.E., Avis, J.D., Belanger, D.W., Thury, M., 1987. Analysis and interpretation of borehole hydraulic tests in deep boreholes – principles, model development, and applications. Water Resour. Res. 23 (7), 1341–1375.
Runchal, A., Maini, T., 1980. The impact of a high-level nuclear waste repository on the regional groundwater-flow. Int. J. Rock Mech. Min. 17 (5), 253–264.
Shepard, D., 1964. A Two Dimensional Interpolation Function for Irregulallry Data Spaced, ACM Nat. Conf., pp. 517–524.
Tiren, S.A., Askling, P., Wanstedt, S., 1999. Geologic site characterization for deep nuclear waste disposal in fractured rock based on 3D data visualization. Eng. Geol. 52 (3–4), 319–346.
Wackernagel, H., 1998. Multivariate Geostatistics: An Introduction With Applications. Springer-Verlag, Berlin.
Wang, M.Y., Kulatilake, P.H.S.W., 2008. Understanding of hydraulic properties from configurations of stochastically distributed fracture networks. Hydrol. Process. 22 (8), 1125–1135.
Yeh, T.C.J., Liu, S.Y., 2000. Hydraulic tomography: development of a new aquifer test method. Water Resour. Res. 36 (8), 2095–2105.
Zhu, J.F., Yeh, T.C.J., 2005. Characterization of aquifer heterogeneity using transient hydraulic tomography. Water Resour. Res. 41 (7).
Zimmerman, R.W., Bodvarsson, G.S., 1996. Hydraulic conductivity of rock fractures. Transport Porous Med. 23 (1), 1–30.